



## Impedance spectroscopy and dielectric studies of nanocrystalline iron doped barium strontium titanate ceramics

Reenu Jacob<sup>1,\*</sup>, Harikrishnan G. Nair<sup>2</sup>, Jayakumari Isac<sup>2</sup>

<sup>1</sup>Department of Physics, CMS College, Kottayam, India

<sup>2</sup>Centre for Condensed Matter, Department of Physics, CMS College, Kottayam, India

Received 17 March 2015; Received in revised form 12 May 2015; Received in revised form 9 June 2015;

Accepted 18 June 2015

### Abstract

Barium titanate compounds have great research attention due to their good electric and in some case interesting magnetic properties. The synthesis and characterization of iron doped barium strontium titanate (BSFTO) make an attempt to understand its structure and investigate electric/dielectric properties. The formation of a perovskite compound with tetragonal phase was confirmed through X-ray structural studies. Dielectric and electrical impedance properties of the sintered BSFTO ceramics were measured in the frequency range from 42 Hz to 2 MHz and at different temperatures (up to 600 °C). It was shown that the properties of this material are highly dependent on temperature and frequency. The nature of frequency dependence of AC conductivity confirms the Jonscher's power law. The temperature dependence of DC conductivity obeys the Arrhenius behaviour.

**Keywords:** X-ray diffraction, dielectric properties, electrical impedance, conductivity

### I. Introduction

Barium titanate compounds are the best known perovskite ferroelectric compounds. They are extensively studied [1,2] due to their peculiarity to accommodate different types of dopants. This opened gates for doped nanosized barium titanate materials for specific technological applications, such as capacitors, sensors with positive temperature coefficients of resistivity, piezoelectric transducers and ferroelectric thin-film memories. Different dopants can be accommodated in the lattice. The ionic radius is the main factor that decides the substitution site for the dopants. SrTiO<sub>3</sub>, BaTiO<sub>3</sub>, KNbO<sub>3</sub>, etc., represent important class of perovskite materials with high potential for future application in microelectronic. Introduction of extrinsic and intrinsic dopants, such as transition metal cations, usually cause formation of cation or oxygen vacancies and, thus, might enhance the properties dramatically [1].

Relaxor ferroelectrics characterized by their broad dielectric transition, also known as the diffused phase transitions, are important materials for use in

non-volatile memory devices. In order to develop environment-friendly materials, efforts are focused on the lead-free materials [2,3]. It is reported that BaTiO<sub>3</sub> has the ferroelectric to paraelectric transition at about 120 °C with very high dielectric constant. To enrich the quality and applications of BaTiO<sub>3</sub> new ceramic material, iron doped barium strontium titanate (BSFTO), was synthesized and studied [4]. In this paper, dielectric and impedance properties of the sintered BSFTO ceramics were investigated in the frequency range from 42 Hz to 2 MHz and at different temperatures (up to 600 °C).

### II. Experimental

Iron doped barium strontium titanate (BSFTO) was prepared by the solid state reaction method initiated by intensive milling in high-energy ball mill followed by attrition milling. The BSFTO sample was prepared from the reagent grade chemicals of high purity. Barium carbonate, strontium carbonate, ferric oxide and titanium dioxide powders were used as the raw materials and weighed according to the cation Ba : Sr : Fe : Ti molar ratio of 1 : 0.6 : 0.4 : 1. The sample after ball milling for three weeks with suitable zirconium balls was attrition milled again for three hours. The obtained powder was

\*Corresponding author: tel: +919496935890, fax: 04812565002, e-mail: reenujacob12@gmail.com

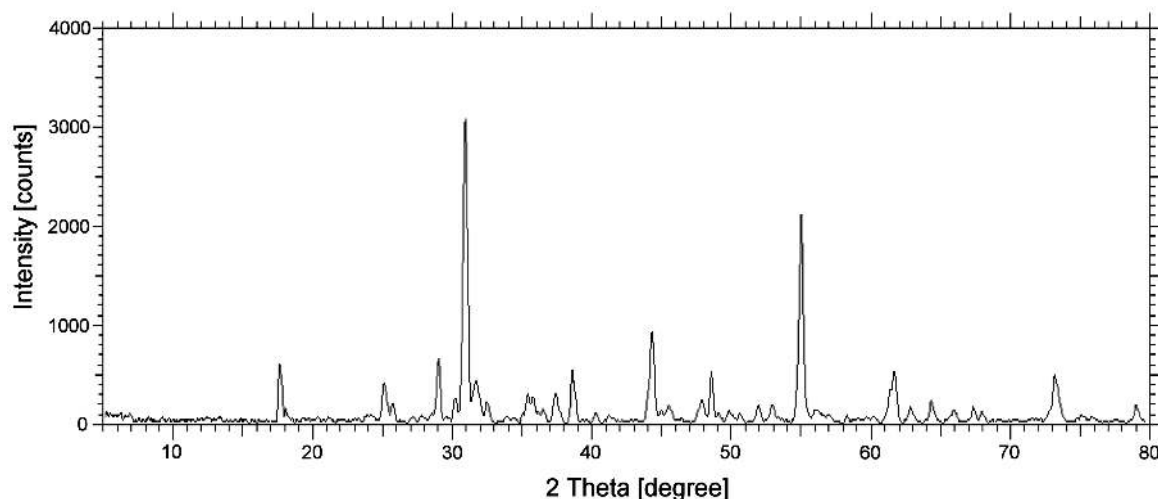


Figure 1. X-ray diffraction pattern of the sample BSFTO at 950 °C

Table 1.  $2\theta$  values and corresponding  $hkl$  lines

$2\theta$ [°]	$hkl$
30.936	115
32.472	106
35.267	302
40.318	304
44.356	302
52.001	316
55.046	414
61.719	0011

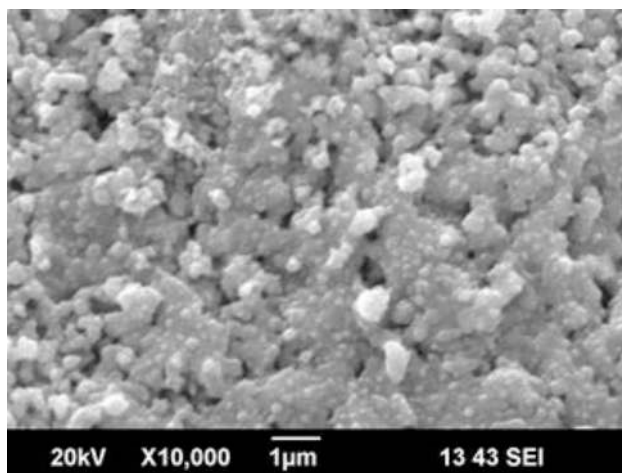


Figure 2. SEM micrograph of the BSFTO sample

then calcined at different temperatures, up to 950 °C, in a special furnace with continuous oxygen flow. The pre-sintered mixture was ground and pressed into pellets of 9.27 mm diameter with 3.07 mm thickness under 300 MPa. The pellets were sintered at 1100 °C for 4 hours and finally cooled to room temperature.

Phase composition of the prepared BSFTO samples was determined using X-ray diffraction on Bruker AXS D8 advance diffractometer and microstructure of the BSFTO ceramics was investigated with SEM (JEOL).

The sintered pellets were plated using air-drying silver paste to ensure good contacting. The electrical mea-

surements were carried out by inserting the sample between two parallel plate conductors forming cell capacitor. The whole arrangement was placed in non-inductive furnace for heating at different temperatures. The variation of dielectric constant, loss tangent and electrical conductivity in the frequency range from 42 Hz to 2 MHz and the temperature range from 30 °C to 600 °C were studied. These measurements were performed on HIOKI-3532-50 LCR Hi Tester.

### III. Results and discussion

#### 3.1. XRD analysis

Figure 1 shows the X-ray diffraction pattern of the BSFTO sample calcined at 950 °C. Crystal structure was solved by analysing the intensities of diffracted X-ray beams using the XPERT-PRO software. From the  $hkl$  values and XRD data cell dimensions were calculated:  $a = 10.2177 \text{ \AA}$ ,  $b = 10.2177 \text{ \AA}$ ,  $c = 5.5167 \text{ \AA}$  and  $\alpha = \beta = \gamma = 90^\circ$ . Thus, the analysis confirmed that this crystal belongs to the tetragonal perovskite system. Positions of the characteristic XRD peaks are given in Table 1. Secondary phase formation peaks were also observed within the detection limits of the XRD. The secondary phase formations in simple perovskite system confirmed the transient intermediate phase during the mixed-oxide processing of Ba- and Ti-containing perovskite materials. X-ray diffraction profile was also used to measure the average crystallite size of the sample provided the average diameter was less than 300 Å. Thus, the crystallite size calculated using Scherrer equation as already reported was found to be 27.5 nm [4].

SEM micrograph (Fig. 2) gave the surface morphology of the sample and confirmed presence of fine structure already indicated with the XRD data.

#### 3.2. Dielectric measurements

The dielectric studies with respect to frequency at various temperatures were well studied. The dielectric constant ( $\epsilon_r$ ) and dielectric loss ( $\tan \delta$ ) of the sintered

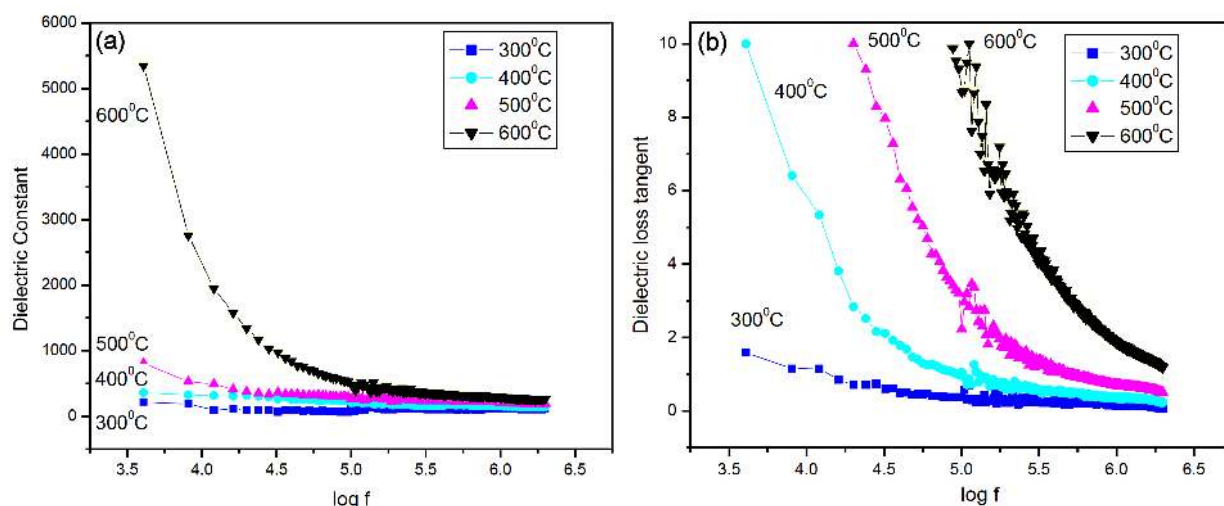


Figure 3. Frequency dependence plot of: a) dielectric constant and b) dielectric loss for different temperatures

BSFTO ceramics exhibited strong dependence on frequency (Fig. 3). The occurrence of dispersion in the low frequency region could be explained with the interfacial polarization. This also confirmed the presence of DC conductivity in the sample [21].

The values of dielectric constant for Fe-doped barium titanate materials were lower compared to the pure barium titanate sample [9,10]. The dielectric studies also confirmed a shift in the transition temperature ( $T_C$ ) towards the lower temperature region with the increase in addition of Fe. The value of ( $T_C$ ) decreased due to the addition of  $Fe^{+3}$  ions, as the lower valence state of  $Fe^{+3}$  ion created an oxygen vacancy breaking the vibration of the Ti–O chains [1]. Another interpretation for such decrease points to the fact that iron oxide has different lattice constant which add a stress in to the lattice [11].

### 3.3. Impedance spectroscopy studies

The complex impedance technique was employed to study the electrical response or transport properties of the sintered BSFTO material in a large frequency range. This can also be used to separate the contributions of electrical properties due to the grains, grain boundaries and electrode/sample interface in a polycrystalline material. If  $Z'$ ,  $M'$ ,  $\epsilon'$ ,  $Y'$  and  $Z''$ ,  $M''$ ,  $\epsilon''$ ,  $Y''$  are the real and imaginary components of the complex impedance, electric modulus, permittivity and admittance then  $\tan \delta = \epsilon''/\epsilon' = M''/M' = -Z''/Z' = Y''/Y'$ . The complex electric modulus is defined by the reciprocal of the complex permittivity. Hence, the complex electric modulus  $M$  reflects the dynamic properties of the sample alone.

The change of  $Z'$ ,  $M'$ ,  $Z''$ ,  $M''$ ,  $\epsilon'$  and  $\epsilon''$  with frequency at different temperatures (as in Fig. 4) showed that impedance varies with the increase in both frequency and temperature. The distinct behaviour becomes prominent at temperature higher than 400 °C in all the cases. This confirmed that the sample tends to be conductive. At higher frequencies  $Z'$  (or  $M'$ ) attains a maximum value ( $Z'_{max}$  or  $M'_{max}$ ) known as relaxation

frequency ( $f_r$ ). The relaxation process occurs due to the presence of immobile charges at lower temperatures, and also due to defects and vacancies at higher temperatures [13]. The variation of imaginary electrical modulus ( $\epsilon''$ ) and imaginary impedance ( $Z''$ ) with frequency at different temperatures for the BSFTO ceramics distinguishes whether relaxation process is due to short range or long range motion of charge carriers. The same concept can also be studied through the admittance ( $Y$ ) plots in function of frequency (Figs. 4g,h).

The peaks of imaginary component of the complex impedance and electric modulus ( $Z''_{max}/Z'_{max}$ ), observed in Figs. 4b,d, shift towards higher frequency range on increasing temperature. The change in the peak position and broadening again confirmed the relaxation processes in the ceramic sample [22]. The relaxation effect and asymmetric peak broadening showed the presence of non-Debye type of relaxation [14]. The obtained plots (Figs. 4b,d) show an asymmetric behaviour with respect to peak maxima whose positions are again frequency and temperature dependent. These curves describe two apparent relaxations — the left region of the peak indicates the conduction process, while the right region indicates the localized motion of ions. The peak shifts towards higher frequency exhibiting the correlation between the motions of mobile charge carriers. The nature of modulus spectrums confirms the existence of hopping mechanism in the electrical conduction of the materials [20]. The angular frequency  $\omega_m$  ( $\omega = 2\pi f$ ), corresponding to  $Z''_{max}$ , gives the most probable relaxation time  $\tau_m$  by the condition  $\omega_m \tau_m = 1$ .

### 3.4. Cole-Cole plot

Real materials show a deviation from the ideal equations and exhibit a non-Debye dielectric behaviour. The non-Debye dielectric response can be described using Cole-Cole/Davidson-Cole and empirical expressions (Fig. 5). The complex impedance plots show semi-circular arcs resolving at high temperature. These asymmetric arcs confirm the existence of non-Debye type of

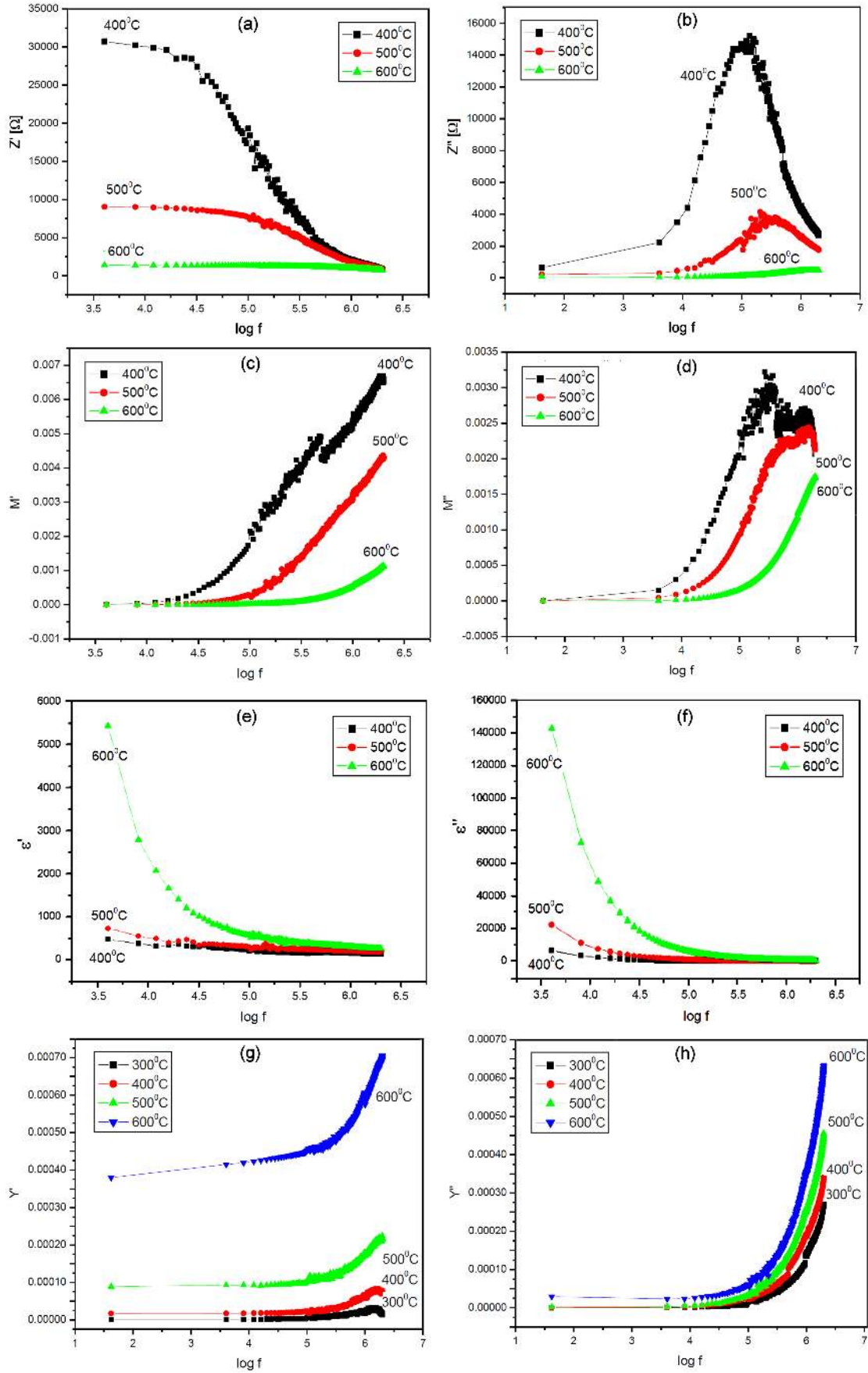


Figure 4. Variation of  $Z'$  (a),  $Z''$  (b),  $M'$  (c),  $M''$  (d),  $\epsilon'$  (e),  $\epsilon''$  (f),  $Y'$  (g) and  $Y''$  (h) with frequency in different temperature range

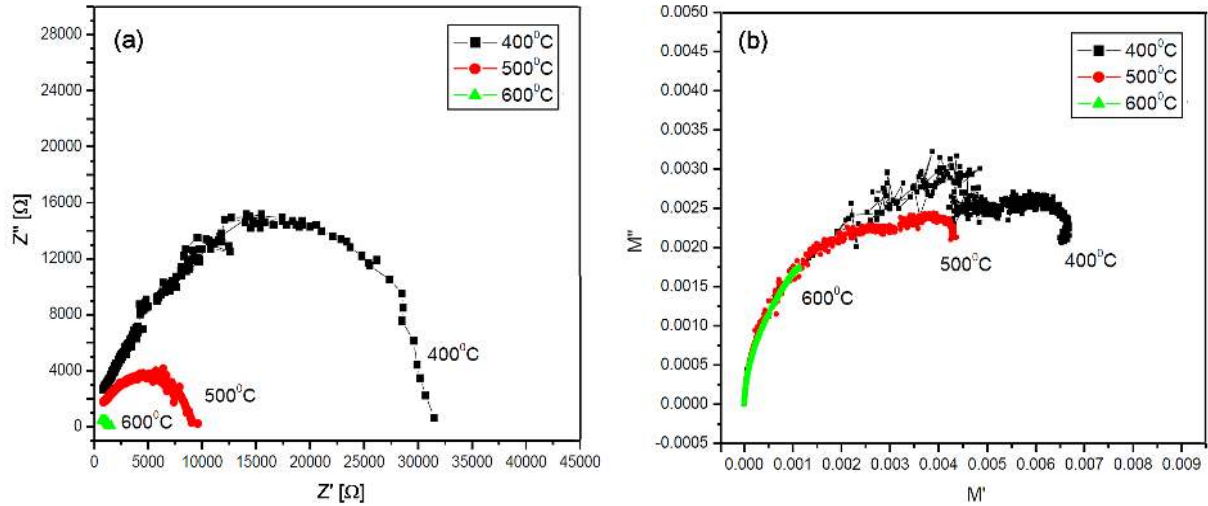


Figure 5. Cole-Cole plots: a)  $Z'$  vs  $Z''$  and b)  $M'$  vs  $M''$

relaxation in the sintered BSFTO sample [16]. The depressed semicircle corresponds to the parallel combination of resistance and capacitance. The plot also suggests that the electrical response consist of two semicircles due to bulk property of the sample and also due to the presence of grain boundary [17]. This nature of decrease in resistance/impedance confirms the negative-temperature coefficient of resistance (NTCR) property characteristic of semiconductors [18].

### 3.5. Activation energy

The temperature dependence of all thermally activated processes can be represented by a general equation of the form:

$$z = A_0 \exp\left(\frac{-E_a}{RT}\right) \quad (1)$$

where  $z$  is the phenomenon that is thermally activated,  $E_a$  the activation energy for the process,  $A_0$  a constant, sometimes called the “pre-exponential constant”,  $R$  universal gas constant ( $8.314 \text{ J} \cdot \text{mol}^{-1} \text{ K}^{-1}$ ) and  $T$  absolute

temperature. Arrhenius plot,  $\ln(z)$  vs.  $(1/T)$ , is usually used for determination of the activation energy and pre-exponential constant in Eq. 1 from the slope and intercept of the best-fit line through the data. Arrhenius plots of  $\log \omega_m$  with the imaginary part of electric modulus and impedance are presented in Fig. 6. The activation energies  $E_a$ , calculated from the linear fit, are 1.78 eV and 1.15 eV for  $Z''$  and  $M''$  variation, respectively.

### 3.6. Conductivity studies – AC conductivity

Study of AC electrical conductivity gives a good quality check on the electrical transport properties of a material by using Jonscher’s power law:

$$\sigma_{AC}(\omega) = \sigma_{DC} + A\omega^n \quad (2)$$

where  $\sigma_{DC}$ , is frequency independent conductivity (frequency independent plateau in the low frequency region),  $A$  the temperature dependent pre-exponential factor and  $n$  the frequency exponent (takes values between 0 and 1). The frequency exponent  $n$  is frequency in-

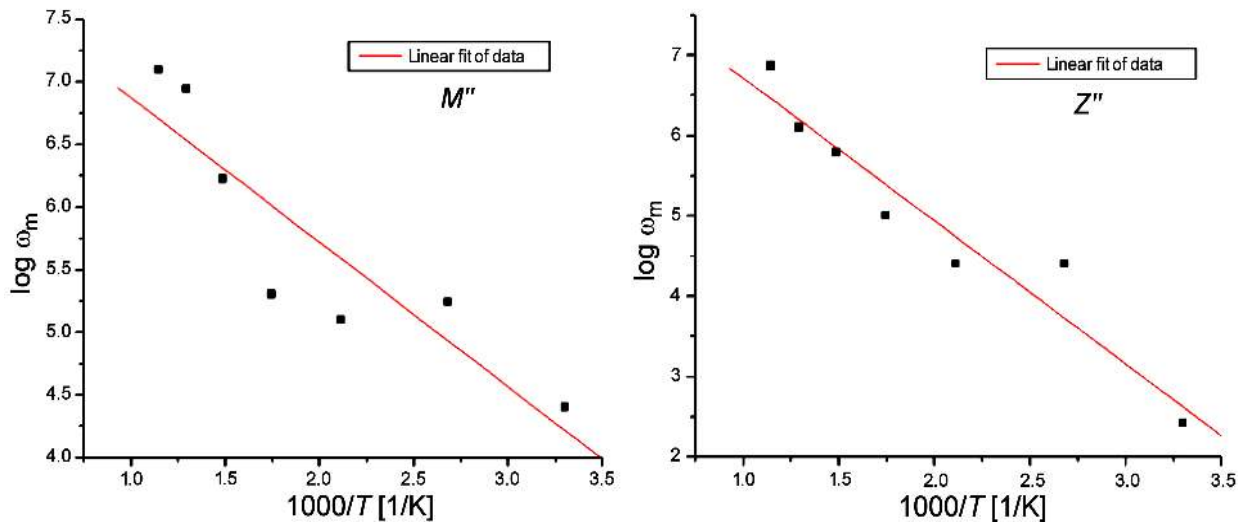


Figure 6. Arrhenius plot of  $\log \omega_m$  with the imaginary part of electric modulus  $M''$  (a) and impedance  $Z''$  (b)

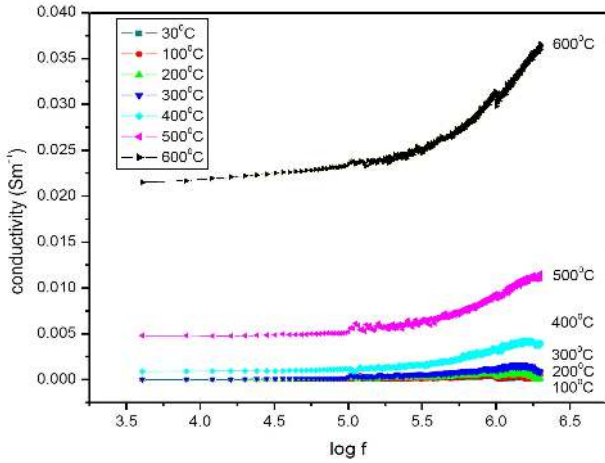


Figure 7. AC conductivity versus frequency graph

dependent, but temperature and material dependent parameter. The experimental  $\sigma_{AC}$  values of the BSFTO ceramics prove Jonscher’s power law as given in Fig. 7. The conductivity graphs clearly indicate three regions: i) dispersion in the low frequency area, ii) an intermediate plateau and iii) conductivity dispersion at high frequency region. Thus,  $\sigma_{AC}$  is independent of frequency in the low frequency region which is generally known as hopping frequency, but shifts towards higher-frequency side with the increase of temperature, as already reported [19]. The increasing value of  $\sigma_{AC}$  with frequency rise is due to the disordering of cations between neighbouring sites, and presence of space charge. The dispersion gets narrowed as frequency is increased. Also conductivity rise with temperature points to a thermally activated process.

### 3.7. Conductivity studies – DC conductivity

Figure 8 shows the variation of  $\sigma_{DC}$  as a function of inverse absolute temperature. The value of bulk conductivity of the sample at different temperatures is obtained from the  $\sigma_{AC}$  plot of the sample by theoretical fitting using Joncher’s power law. The DC conductivity of the BSFTO material shows almost a linear rise with temperature, exhibiting the negative temperature coefficient of resistance (NCTR) behaviour. At higher temperature,

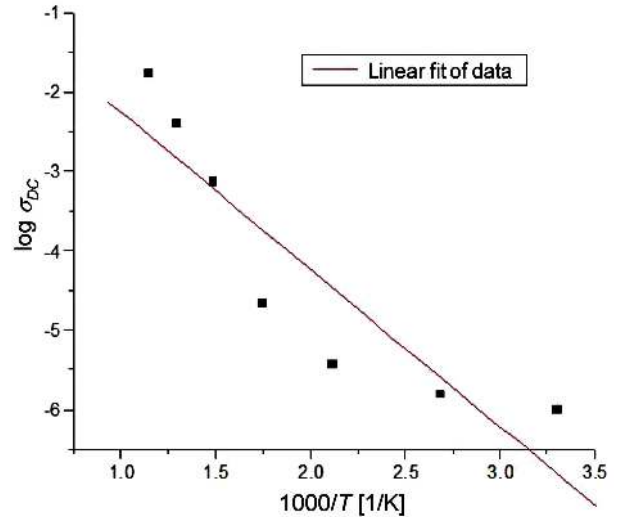
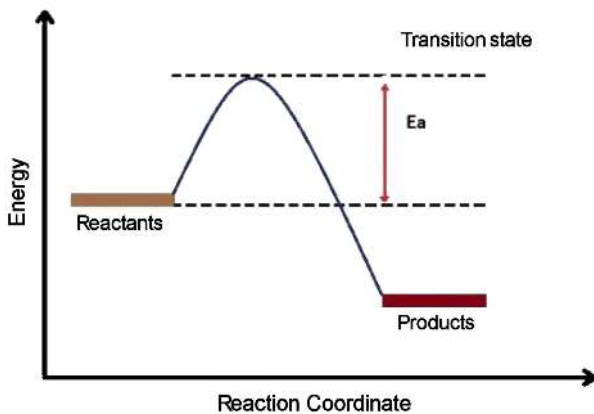


Figure 8.  $\sigma_{DC}$  as a function of inverse of absolute temperature (slope gives the activation energy as 1.97 eV)

the conductivity versus temperature response can be explained by a thermally activated transport of Arrhenius type.

According to the kinetic theory of gas as temperature increases, gas molecule velocity also increases. Thus, the fraction of molecules that have high enough kinetic energy to overcome the energy barrier also increases. The fraction of molecules with energy equal to or greater than  $E_a$  (activation energy) is given by the Arrhenius relation:

$$\sigma_{DC} = \sigma_0 + e^{-\frac{E_a}{k_B T}} \quad (3)$$

where  $\sigma_0$  is frequency factor constant or also known as pre-exponential factor or Arrhenius factor which gives the rate of collision and the fraction of collisions with the proper orientation for the reaction to occur. As it can be seen in Fig. 9, the reaction of  $E_a$  has a strong dependence on temperature. The conductivity response curve can be attributed to Mott’s hopping type phenomena. The  $\sigma_{DC}$  activation energy of the material is found to be equal to 1.97 eV. The activation energy values (from  $\sigma_{DC}$  and electrical impedance data) confirm the hopping mechanism in the investigated BSFTO material.

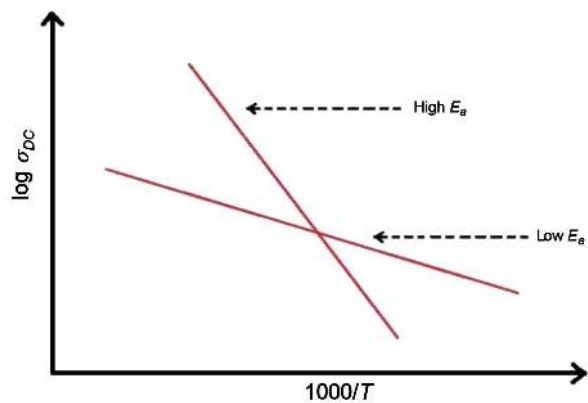


Figure 9. Activation energy reaction rates with temperature

#### IV. Conclusions

Structural and electrical study of iron doped barium strontium titanate (BSFTO) ceramics was successfully done. Results showed interesting dielectric and impedance characteristics. The grain conduction and relaxation of the sample evaluated from Cole-Cole plots gave clear confirmatory results. The anomaly in dielectric properties of doped BSFTO in the temperature range 350–450 °C showed a pure phase transition. The impedance data indicate that the relaxations in the samples are due to the presence of polarizing species. The polarizing charges give non-Debye relaxations and contribute to grain boundary capacitance and conductance. The  $\sigma_{AC}$  conductivity plots well confirm the Jonscher's power law. The temperature dependence of DC conductivity studied through the Arrhenius equation proves the hopping mechanism in the sample. The presence of Fe cations results in the reduction of dielectric properties throwing light to the high conductive scope for the material. Thus, the prepared lead-free BSFTO ceramics will have promising future in areas of piezoelectricity, pyroelectricity and optical frequency doubling effects.

**Acknowledgements:** The authors are grateful to SAIF, Kochi for providing the instrumental data, UGC and to the Principal, CMS College, Kottayam, Kerala for providing the necessary facilities.

#### References

1. A. Mishra, N. Mishra, "Iron-doped BaTiO<sub>3</sub>: Influence of iron on physical properties", *Int. J. Mater. Sci. Appl.*, **1** [1] (2012) 14–21.
2. M. Mahesh Kumar, M.B. Suresh, S.V. Suryanarayana, G.S. Kumar, T. Bhimasankaram, "Dielectric relaxation in Ba<sub>0.96</sub>Bi<sub>0.04</sub>Ti<sub>0.96</sub>Fe<sub>0.04</sub>O<sub>3</sub>", *J. Appl. Phys.*, **84** (1998) 6811–6814.
3. M. Mahesh Kumar, M.B. Suresh, S.V. Suryanarayana, "Electrical and dielectric properties in double doped BaTiO<sub>3</sub> showing relaxor behavior", *J. Appl. Phys.*, **86** [3] (1999) 1634–1637.
4. R. Jacob, J. Isac, "X-ray diffraction line profile analysis of BaSr<sub>0.6</sub>Fe<sub>0.4</sub>TiO<sub>3</sub> [BSFTO]", *Int. J. Chem. Studies*, **2** [5] (2015) 12–21.
5. A.R. West, *Solid State Chemistry and its Applications*, John Wiley & Sons, New York, 1987.
6. A. Shukla, R.N.P. Choudhary, "Study of aliovalent modification on dielectric and ac conductivity properties in lead titanate nanoceramics", *J. Mater. Sci.: Mater. Electron.*, **22** (2011) 1222–1228.
7. J. Rout, R. Padhee, P.R. Das, R.N.P. Choudhary, "Structural, dielectric and electrical properties of BiFeW<sub>2</sub>O<sub>9</sub> ceramics", *Adv. Appl. Phys.*, **1** [3] (2013) 105–116.
8. P. Venkateswarlu, A. Laha, S.B. Krupanidhi, "AC properties of laser ablated La-modified lead titanate thin films", *Thin Solid Films*, **474** (2005) 1–9.
9. R. Vivekanandan, T.R.N. Kuty, "Hydrothermal synthesis of Ba(Ti,Sn)O<sub>3</sub> fine powders and dielectric properties of the corresponding ceramics", *Ceram. Int.*, **14** (1988) 207–206.
10. G. Arlt, D. Henningsand, G. de With, "Dielectric properties of fine grained barium-titanate ceramics", *J. Appl. Phys.*, **58** (1985) 1619–1625.
11. M. Willander, O. Nur, M.Q. Israr, A.B. Abou Hamad, F.G. El Desouky, M.A. Salem, I.K. Battisha, "Determination of A.C. conductivity of nanocomposite perovskite Ba<sub>(1-x-y)</sub>Sr<sub>(x)</sub>TiFe<sub>(y)</sub>O<sub>3</sub> prepared by the sol-gel technique", *J. Crystal. Process Technol.*, **2** (2012) 1–11.
12. P. Ganguly, A.K. Jha, K.L. Deori, "Complex impedance studies of tungsten-bronze structured Ba<sub>5</sub>SmTi<sub>3</sub>Nb<sub>7</sub>O<sub>30</sub> ferroelectric ceramics", *Solid State Commun.*, **146** (2008) 472–477.
13. C.K. Suman, K. Prasad, R.N.P. Choudhary, "Complex impedance studies on tungsten-bronze electroceramic: Pb<sub>2</sub>Bi<sub>3</sub>LaTi<sub>5</sub>O<sub>18</sub>", *J. Mater. Sci.*, **41** (2006) 369–375.
14. S. Sen, R.N.P. Choudhary, "Impedance studies of Sr modified BaZr<sub>0.05</sub>Ti<sub>0.95</sub>O<sub>3</sub> ceramics", *Mater. Chem. Phys.*, **87** (2004) 256–263.
15. J. Plochanski, W. Wiczoreck, "Impedance spectroscopy and phase structure of PEO-NaI complexes", *Solid State Ionics*, **28-30** (1982) 1014–1017.
16. B. Behera, P. Nayak, R.N.P. Choudhary, "Impedance spectroscopy study of NaBa<sub>2</sub>V<sub>5</sub>O<sub>15</sub> ceramic", *J. Alloys Compd.*, **436** (2007) 226–232.
17. B.N. Parida, Piyush R. Das, R. Padhee, R.N.P. Choudhary, "A new ferroelectric oxide Li<sub>2</sub>Pb<sub>2</sub>Pr<sub>2</sub>W<sub>2</sub>Ti<sub>2</sub>Nb<sub>2</sub>O<sub>30</sub>: Synthesis and characterization", *J. Phys. Chem. Solids*, **73** (2012) 713–719.
18. C. Karthik, B.R. Varma, "Dielectric and AC conductivity behavior of BaBi<sub>2</sub>Nb<sub>2</sub>O<sub>9</sub> ceramics", *J. Phys. Chem. Solids*, **67** (2006) 2437–2441.
19. I. Rivera, A. Kumar, N. Ortega, R.S. Katiyar, S. Lushnikov, "Divide line between relaxor, diffused ferroelectric, ferroelectric and dielectric", *Solid State Commun.*, **149** [3-4] (2009) 172–176.
20. S. Sahoo, U. Dash, S.K.S. Parashar, S.M. Ali, "Frequency and temperature dependent electrical characteristics of CaTiO<sub>3</sub> nano-ceramic prepared by high-energy ball milling", *J. Adv. Ceram.*, **2** [3] (2013) 291–300.
21. M.R. Biswal, J. Nanda, N.C. Mishra, S. Anwar, A. Mishra, "Dielectric and impedance spectroscopic studies of multiferroic BiFe<sub>1-x</sub>Ni<sub>x</sub>O<sub>3</sub> ceramics", *Adv. Mater. Lett.*, **5** [9] (2014) 531–537.
22. B.N. Parida, P.R. Das, R. Padhee, R.N.P. Choudhary, "Synthesis and characterization of tungsten bronze ferroelectric oxide", *Adv. Mater. Lett.*, **3** [3] (2012) 231–238.

